Available online at www.sciencedirect.com

ScienceDirect

Ceramics International 40 (2014) 5801–5809

CERAMICS INTERNATIONAL

www.elsevier.com/locate/ceramint

Investigation of 30-cell solid oxide electrolyzer stack modules for hydrogen production

Yifeng Zheng, Qingshan Li, Wanbin Guan, Cheng Xu*, Wei Wu, Wei Guo Wang**

Division of Fuel Cell and Energy Technology, Ningbo Institute of Material Technology and Engineering (NIMTE), Chinese Academy of Sciences, Ningbo 315201, PR China

Received 26 October 2013; received in revised form 1 November 2013; accepted 1 November 2013
Available online 12 November 2013

Abstract

The 30-cell nickel-yttria stabilized zirconia (Ni-YSZ) hydrogen electrode-supported planar solid oxide electrolyzer (SOE) stack modules were manufactured and tested at 800 °C in steam electrolysis mode for hydrogen production. The electrolysis efficiency of the stack modules was higher than 100% at a total steam and hydrogen flow of 2.1 sccm cm^{-2}, a H_2O/H_2 ratio of 80/20, and a current density of <0.2 A cm^{-2}. The electrolysis efficiency, current efficiency, and actual hydrogen production rate of the stack modules increased with increasing H_2O/H_2 ratio at a constant current density. However, the electrolysis and current efficiencies decreased steadily at high current densities. During hydrogen production, the stack modules were operated at 800 °C and a constant current density of 0.15 A cm^{-2} for up to 1100 h. A steam conversion rate of 62% and current efficiency of 87.4% were obtained; the actual hydrogen production rate reached as high as 103.6 N L h^{-1}. Post-mortem analysis showed that delamination of the LSM–YSZ oxygen electrode mainly occurred in the steam and air inlet area of the 10×10 cm^2 cells.

Keywords: Solid oxide electrolyzer cell; Hydrogen production; 30-Cell stack; Electrolysis efficiency; Current efficiency

1. Introduction

Clean and efficient methods of hydrogen production are required for economic application. At present, steam reformation from methane is the primary method by which hydrogen is produced. Unfortunately, this method also increases carbon emissions in the atmosphere. A recent research has focused on sustainable and green methods, such as gasification of biomass, photocatalytic water splitting, and water electrolysis driven by solar cells or wind turbines [1–3]. Water electrolysis is an especially practical and efficient method for hydrogen production. Compared with ordinary alkaline water electrolysis, steam electrolysis in solid oxide electrolyzer cells (SOECs) operating at high temperatures consumes less electrical energy and is more efficient for hydrogen production [4–8]. Moreover, the heat and power generated by nuclear power, renewable energy, and waste heat from high-temperature industrial processes can be utilized for steam electrolysis in SOECs to achieve even higher efficiency [9].

In an SOEC, steam is supplied to the hydrogen electrode side of the cell as a reactant and oxygen ions are transported to the oxygen electrode through the electrolyte. Hydrogen is then produced at the hydrogen electrode side. An SOEC undergoes essentially the reverse process of a solid oxide fuel cell (SOFC). Thus, SOEC technology can be built based on the extensively researched SOFC technology [5,10]. Two basic designs for SOEC development are currently available – electrolyte-supported cells and electrode-supported cells [11,12]. In electrolyte-supported cells, while the ohmic resistance of the electrolytes limits the overall cell performance because of the thickness of the electrolyte, which is typically over 100 μm, such cells are usually suitable for operation at high temperatures (such as 1000 °C). In electrode-supported cells, the electrolyte thickness can be decreased to 10–20 μm, significantly decreasing the ohmic resistance of the cells

*Corresponding author. Tel.: +86 574 8668 5139.
**Corresponding author. Tel.: +86 574 8791 1363.
E-mail addresses: xucheng@nimte.ac.cn (C. Xu), wgwang@nimte.ac.cn (W.G. Wang).

0272-8842/$ - see front matter © 2013 Elsevier Ltd and Techna Group S.r.l. All rights reserved.
http://dx.doi.org/10.1016/j.ceramint.2013.11.020

[13,14]. Electrode-supported cells, such as hydrogen electrode-supported SOECs based on cell assemblies composed of nickel-yttria stabilized zirconia (Ni-YSZ) hydrogen electrode/YSZ electrolyte/lanthanum strontium manganite–YSZ (LSM–YSZ) oxygen electrode [15–17], are more suitable for operation at intermediate temperature (600–800 °C) applications than electrolyte-supported cells.

Most studies on SOEC technology have focused on the electrolysis performance and degradation of single SOEC cells as well as SOEC material development [5,18]. A limited number of studies have been performed on the performance and durability of SOE stacks. The Idaho National Laboratory recently studied the large-scale production of hydrogen from nuclear energy [9] using externally manifolded stacks with three modules based on electrolyte-supported cells; however, the research group concerned observed significant performance degradation. Petitjean et al. [19] evaluated short stacks based on standard SOFC Ni-YSZ supported cells. Durability tests were carried out for 2700 h on these cells at 800 °C with a current density of 0.5 A cm^{-2} and a steam conversion rate of 25% in SOEC mode; however, significant long-term performance degradation ($>5\%\ kh^{-1}$) was also found. Kim et al. [6] used a three-cell flat-tubular SOE stack for hydrogen production and obtained a hydrogen production rate of 4.1 L h^{-1} at an average current density of approximately 0.11 A cm^{-2}. The Ningbo Institute of Material Technology and Engineering (NIMTE) of the Chinese Academy of Sciences has also developed stacks for SOFC applications [20,21] and showed the feasibility of using these stacks in SOEC mode for hydrogen production for up to 1000 h [22].

Several research studies have been conducted on the performance of SOE cells and stacks; however, the performance of these materials is poorer than that of SOFC cells and stacks because the operating conditions of SOECs are generally more severe than those of SOFCs. When an SOEC is operated in multiple-cell stacks for large-scale hydrogen production, factors such as current density, gas flow, and steam molar fraction at the inlet become important [23,24]. Electrolysis and current efficiencies are also associated with SOEC performance. The electrolysis efficiency quantifies the heat value of the hydrogen produced by electrolysis per unit of electrical energy consumed in the stack [25]. According to some studies [6,26], the hydrogen generation rate of SOECs may be calculated from Faraday's law, assuming 100% current efficiency. In fact, the actual current efficiency cannot reach as high as 100% in the stack. However, systematic studies on the influence of different operating conditions on the performance of SOE stacks remain lacking.

The present study aimed to systematically investigate 30-cell SOE stack modules for hydrogen production under different operating conditions. 30-Cell Ni-YSZ hydrogen electrode-supported planar SOE stack modules were manufactured and tested to evaluate the effects of total steam and hydrogen flow in the hydrogen electrode, steam-to-hydrogen ratio, and current density. The electrolysis efficiency, current efficiency, and durability of SOE stack modules operating for up to 1100 h were also evaluated.

2. Experimental

2.1. Fabrication of 30-cell SOE stack modules

The 30-cell SOE stack modules were produced at the NIMTE. Each stack module contained 30-cell planar Ni-YSZ hydrogen electrode-supported single cells and had a total active area of 1890 cm^2. Each single cell in the stack featured a 400 μm thick NiO–YSZ electrode substrate, a 10 μm thick NiO–YSZ electrode functional layer, a 10 μm thick 8YSZ electrolyte layer, and a 30–40 μm-thick LSM–YSZ electrode. The overall single cell area for testing was $10 \times 10\ cm^2$ and the active area was 63 cm^2. In the stack, SUS430 ferritic stainless steel was used to create metal interconnects that were also adopted as co-flow gas channels. Gas flow channels were etched in a 10 mm × 1.5 mm area at the interconnects with a channel tip height of about 0.6 mm. Porous nickel foam was placed on the NiO–YSZ electrode side of the interconnect as the current collecting layer. To prevent high-temperature oxidation and Cr vaporization, the LSM–YSZ electrode side of the interconnect was densely coated with LSM microspherical powders by plasma spraying. LSM particles with diameters of approximately 75 μm were coated on the original LSM–YSZ electrode side to improve the output performance of the stack and individual cells. Other parameters used are listed elsewhere [20,21]. After assembly, the stack was placed in a furnace and heated to 850 °C at a rate of 1 °C min^{-1}. An external weight was loaded on the stack for better sealing. After maintaining the temperature at 850 °C for 4 h, the stack was cooled to room temperature at a ramp rate of 1 °C min^{-1}.

2.2. Performance test of the SOE stack modules

The stack module was mounted into the furnace of a test bench for testing, as shown in Fig. 1. The test bench was equipped with a DC power supply and electronic loads that allowed reversible operation. Before mounting, voltage probes were placed on both sides of the stack module electrode (Fig. 1). The SOE stack module was then heated at a rate of 1 °C min^{-1} until 800 °C. N_2 gas was used to purge and protect the stack module from oxidization during the heating process. After maintaining the stack module at 800 °C for over 60 min,

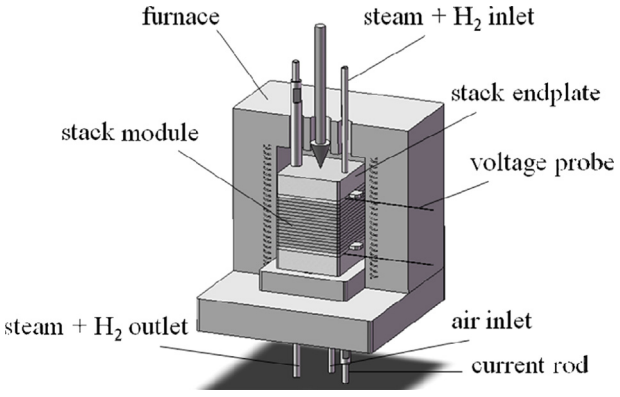

Fig. 1. 3D view of the stack module mounting.

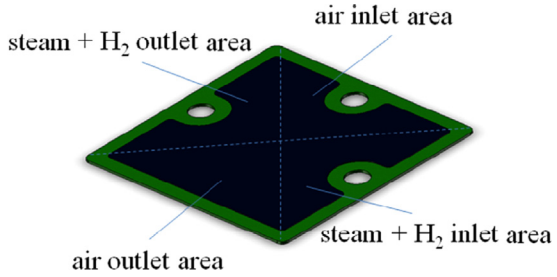

Fig. 2. Different parts of the cells for microstructure characterization.

a certain amount of external pressure was loaded on the stack module to ensure excellent sealing at high temperatures. Hydrogen (2.1 sccm cm^{-2}) and air (6.3 sccm cm^{-2}) were then introduced to the NiO–YSZ hydrogen electrode and the LSM–YSZ oxygen electrode, respectively, of the stack module. The NiO–YSZ electrode was reduced by H_2 at 800 °C for about 5 h before the performance test was performed on the SOE stack.

The electrolysis performance of the SOE stack modules was examined under different H_2O/H_2 ratios and current density values. Current density–voltage (*I–V*) curves under electrolysis mode were recorded during the tests. A long-term durability test in electrolysis mode was performed after initial performance testing. After water vapor condensation and drying, the actual hydrogen production rate at the outflow from the hydrogen electrode of the SOE stack modules was measured by a mass flow controller (MFC) (Beijing Sevenstar Electronics Co., Ltd., China). Finally, the stack modules were cooled from 800 °C to room temperature at a rate of 1 °C min^{-1} with hydrogen to protect the hydrogen electrode from oxidization. The microstructures of the SOECs were observed using a HITACHI S4800 scanning electron microscopy (SEM) system coupled to an energy-dispersive X-ray spectroscopy (EDS) system. Square cells (10 cm × 10 cm) were equally divided into four subparts from the two diagonal parts with steam (steam+H_2) or air inlet area and steam (steam+H_2) or air outlet area (Fig. 2) for characterization.

3. Results and discussion

3.1. Investigation of the SOE stack modules under different operating conditions

In the SOEC tests, a mixture of hydrogen and steam was introduced to the hydrogen electrode side of the electrolysis cells. Hydrogen was used as an inlet carrier gas to facilitate the flow of steam and maintain a reductive environment for the hydrogen electrode. Air was introduced to the oxygen electrode to sweep oxygen generated there. Airflow to the oxygen electrode in the 30-cell SOE stack module was kept constant at 12 L min^{-1} (6.3 sccm cm^{-2}). *I–V* curves of the SOE stack module were recorded for a series of steam and hydrogen concentrations at 800 °C. In SOEC mode, negative current densities indicate the power consumption required to split water for hydrogen and oxygen production.

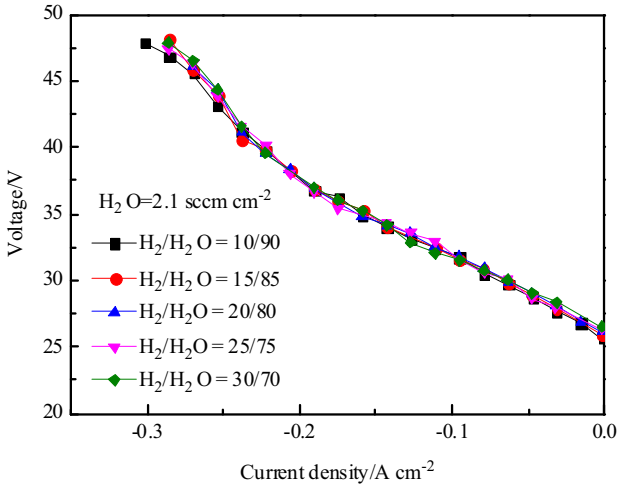

Fig. 3. Effect of different inlet H_2/H_2O ratios on the hydrogen electrode on the *I–V* curves of the stack module at 800 °C and a constant steam flow rate of 2.1 sccm cm^{-2}.

Fig. 3 shows the effect of different inlet H_2/H_2O ratios on the hydrogen electrode on the performance of the stack module at a constant steam value of 2.1 sccm cm^{-2}. No appreciable *I–V* difference was observed as the H_2/H_2O ratio increased from 10/90 to 30/70. Increases in the hydrogen volume fraction had little effect on the stack performance over the current density range under investigation (< 0.3 A cm^{-2}). While the voltage varied linearly at low current densities, distinct steam starvation phenomena at high current densities were observed [27]. Similar slope changes have been reported in other studies [28,29].

Fig. 4a shows the effect of different total steam and hydrogen flows on the hydrogen electrode on the *I–V* polarization curves of the SOE stack module at 800 °C and a constant steam-to-hydrogen ratio (H_2O/H_2=80/20). Fig. 4b shows the corresponding steam conversion rates and electrolysis efficiencies. The steam conversion rate can be calculated using Faraday's law [27,30]. The electrolysis efficiency was calculated based on the following equation [25]:

$$\eta_e = \frac{V_{th}}{V_{op}} \quad (1)$$

where V_{th} is the thermal-neutral voltage of the cell and V_{op} is the cell operating voltage. The thermal-neutral voltage for a single cell is 1.278 V at 800 °C [25]. In Fig. 4a, the current density at a given voltage generally increased with increasing total steam and hydrogen flow. The current density increment was nearly saturated when the total steam and hydrogen flow reached 2.1 sccm cm^{-2}. According to Faraday's law, the amount of hydrogen generated per area by an SOEC is proportional to the current density applied during the electrochemical reaction [17]. Thus, the SOE stack module showed excellent performance under total steam and hydrogen flows of 2.1 and 2.6 sccm cm^{-2}.

In Fig. 4b, the steam conversion rate decreased and the electrolysis efficiency increased with increasing total steam and hydrogen flow. Changes in steam conversion rate

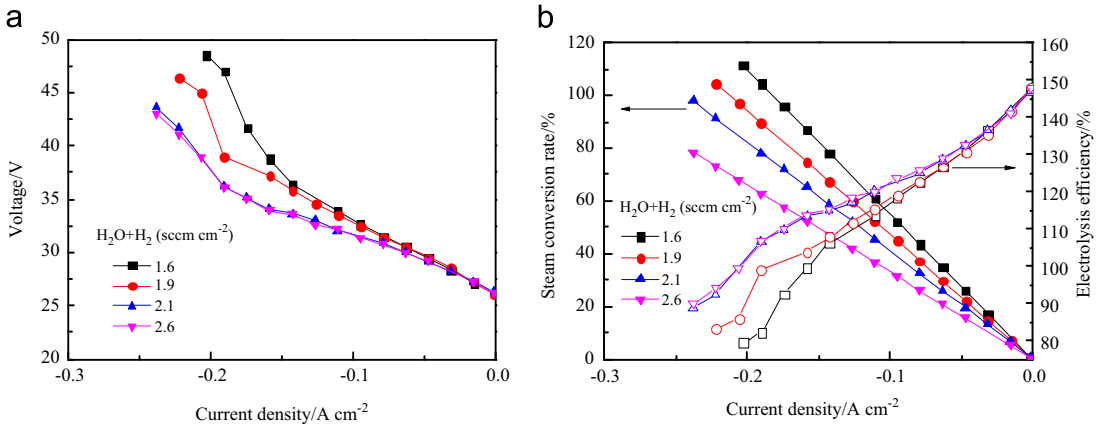

Fig. 4. Effect of different total steam and hydrogen flows on the hydrogen electrode on (a) the *I–V* curves and (b) steam conversion rates and electrolysis efficiencies of the SOE stack module at 800 °C and a constant steam-to-hydrogen ratio (H_2O/H_2=80/20).

contradicted those observed for electrolysis efficiency. The SOEC also operated endothermically under low current densities, which is in accordance with the theory. However, because of large IR losses mainly attributed to electrolyte resistance, the electrolysis efficiency of the stack modules decreased with increasing current density due to the Joule heat [31]. The electrolysis efficiencies obtained under total steam and hydrogen flows of 2.1 and 2.6 sccm cm^{-2} were higher than 100% at current densities < 0.2 A cm^{-2}. The stack module operating under a total steam and hydrogen flow of 2.1 sccm cm^{-2} also achieved a relatively high steam conversion rate (Fig. 4b). These results indicate that a total steam and hydrogen flow of 2.1 sccm cm^{-2} on the hydrogen electrode is suitable for obtaining excellent performance in the present 30-cell SOE stack module (Fig. 4).

The steam-to-hydrogen ratio is generally $> 70\%$ in SOECs [17]. To achieve excellent performance, the *I–V* polarization performance, electrolysis efficiency, and ASR of the SOE stack modules were further investigated by varying the H_2O/H_2 ratio from 70/30 to 90/10 under a total steam and hydrogen flow of 2.1 sccm cm^{-2} (Fig. 5). The slope of the *I–V* curves slightly decreased with increasing H_2O/H_2 ratio (Fig. 5a), and the voltage curves tended to behave linearly at high inlet steam contents. Nonlinearity of the curves at low steam contents is associated with the high sensitivity of the Nernst potential to small changes in average steam content. At an output voltage of 39 V, the current density values were only 0.185 and 0.195 A cm^{-2} at H_2O/H_2 ratios of 70/30 and 75/25; these values increased to 0.206, 0.209, and 0.221 A cm^{-2} at H_2O/H_2 ratios of 80/20, 85/15, and 90/10, respectively. Current densities observed at H_2O/H_2 ratios of 80/20 and 90/10 were relatively higher than those observed at H_2O/H_2 ratios of 70/30 and 75/25. Fig. 5a also shows the electrolysis efficiencies obtained under different H_2O/H_2 ratios. Similar to Fig. 4b, the electrolysis efficiency increased with increasing H_2O/H_2 ratio. In addition, electrolysis efficiencies were higher than 100% at H_2O/H_2 ratios of 80/20 and 90/10 and current densities < 0.2 A cm^{-2}. However, electrolysis efficiencies decreased at higher current densities because of increases in the operating voltage. Such increases are attributed to the larger amount of heat generated from the stack internal resistance than that required for water decomposition at high current densities, which results in the stack operating exothermically.

Fig. 5b shows variations in the ASRs of the stack module with increasing H_2O/H_2 ratios. The ASR represents the net effect of all of the loss mechanisms in the electrolysis stack, including ohmic loss, activation, and concentration overpotentials, among others. If a target current density (and corresponding hydrogen production rate) is selected, lower ASR values allow for stack operation at lower voltages and higher electrolysis efficiencies. The ASR value was calculated based on Ref. [7]. ASR curves presented concave shapes with the lowest values found at current densities between 0.15 and 0.2 A cm^{-2}. The ASR obtained at a H_2O/H_2 ratio of 80/20 was lower than those obtained at H_2O/H_2 ratios of 85/15 and 90/10. Therefore, a H_2O/H_2 ratio of 80/20 was considered the suitable steam-to-hydrogen ratio for the SOE stack module operating at 800 °C. At this ratio, the SOE stack module showed excellent performance with high electrolysis efficiency and low ASR. In the ASR curve obtained at a H_2O/H_2 ratio of 80/20, knee of the curve was found at around 0.15 A cm^{-2} and the steam conversion rate reached as high as 62%. Therefore, to achieve high hydrogen production rates with excellent performance, 0.15 A cm^{-2} was selected as the suitable galvanostatic current density for hydrogen production using SOE stack modules.

3.2. Long term degradation and hydrogen production rate

After the 30-cell SOE stack modules were subjected to initial tests, durability tests under constant galvanostatic electrolysis conditions were conducted. The voltage and current density across the electrolysis stack modules were continuously monitored. Two typical durability curves of the SOE stack modules are shown in Fig. 6a. Galvanostatic electrolysis at 1030 and 255 h were recorded for stack module 1 (from 30 h to 1060 h) and stack module 2 (from 150 to 405 h) at 800 °C and an electrolysis current density of 0.15 A cm^{-2} with a H_2O/H_2 ratio of 80/20. Similar voltage variation curves with time were observed for the two stack modules,

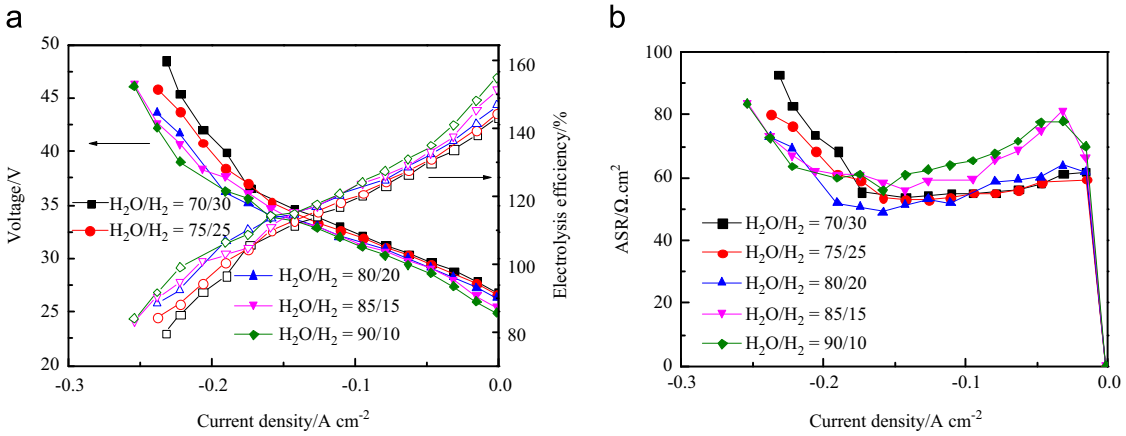

Fig. 5. (a) *I–V* curves and electrolysis efficiencies and (b) ASRs of the SOE stack modules at 800 °C as a function of H_2O/H_2 ratios (70/30–90/10) in the hydrogen electrode with a total steam and hydrogen flow of 2.1 sccm cm^{-2}.

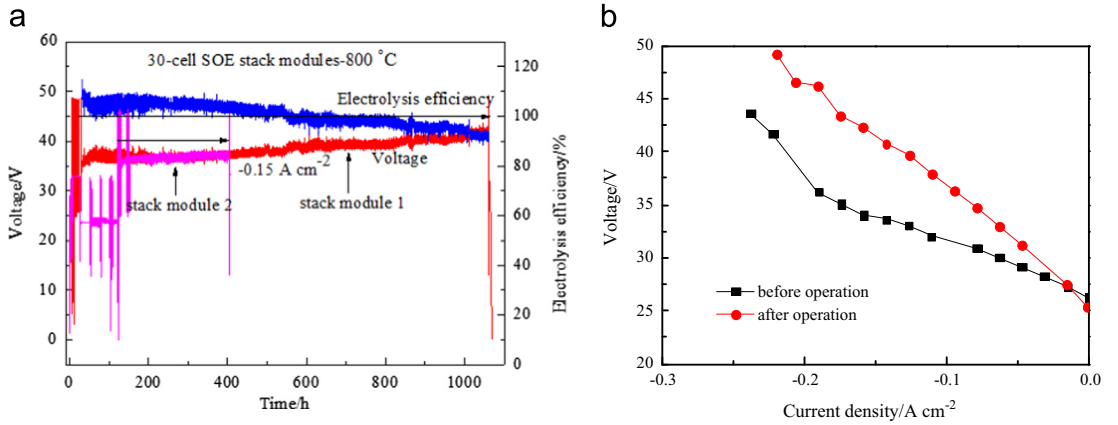

Fig. 6. (a) Durability and electrolysis efficiency of two typical SOE stack modules at 0.15 A cm^{-2} with a H_2O/H_2 ratio of 80/20. (b) *I–V* responses of the stack module before and after operation in constant galvanostatic electrolysis mode for 1030 h.

thus confirming the consistency of the performance of the SOE stack modules. The stack module showed a performance degradation rate of about 12.1% after 1030 h of operation, corresponding to a degradation rate of 11.7% kh^{-1}. This degradation rate is higher than that reported by Schefold et al. [32] (degradation rate = 5.6% kh^{-1} for a five-cell short stack) but within the degradation rates (7% kh^{-1} and 13% kh^{-1} for a short stack) found by Petitjean et al. [19]. The steam conversion rate of the 30-cell stack module was 62%, much higher than that of a short stack (25%) [19]. In addition, the electrolysis efficiency of the stack module decreased from 113% to 92%, as shown in Fig. 6a. The heat value of hydrogen produced by the electrolysis of electrical energy consumed decreased with increasing length of stack module operation. Only part of the electrical energy was converted to hydrogen internal energy after long-term SOE stack operation; hence, the electrolysis efficiency was less than 100%. Fig. 6b shows the *I–V* response of the SOE stack module before and after 1030 h of electrolysis operation. The stack module exhibited an OCV of 26.27 V before operation and an OCV of 25.38 V after 1030 h of operation. Such a finding indicates the development of a sealing leakage after prolonged operation, which could be attributed to the effects of performance degradation of the stack module.

According to Kim et al. [6], based on Faraday's law, the theoretical hydrogen production rate (100% current efficiency) converted from the electronic balance and equivalent hydrogen production can be defined as follows:

$$\dot{n} = \frac{I}{2F} \tag{1}$$

where $\dot{n}$ is the theoretical hydrogen production rate (mol s^{-1}) per cell, I is the input current (A), 2 is the number of electrons involved in the steam electrolysis reaction (the current input corresponding to 2 mol of electrons produces 1 mol of hydrogen molecules), and F is the Faraday constant or the charge of 1 mol of electrons. Using Eq. (1), n for a 30-cell SOE stack module operated at an electrolysis current density of 0.15 A cm^{-2} for 1030 h of galvanostatic electrolysis was calculated to be 1.975 L min^{-1}. The theoretical hydrogen production rate of the stack module was 1.975 L min^{-1} under nominal operating conditions.

The direct hydrogen production rate of the 30-cell SOE stack module was also measured using an MFC. Given that

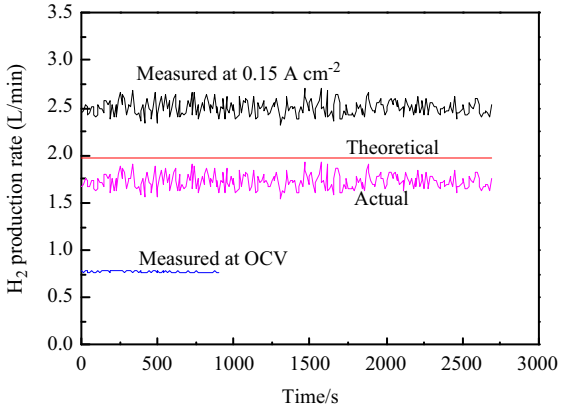

Fig. 7. Hydrogen production performance of the 30-cell SOE stack module at 800 °C.

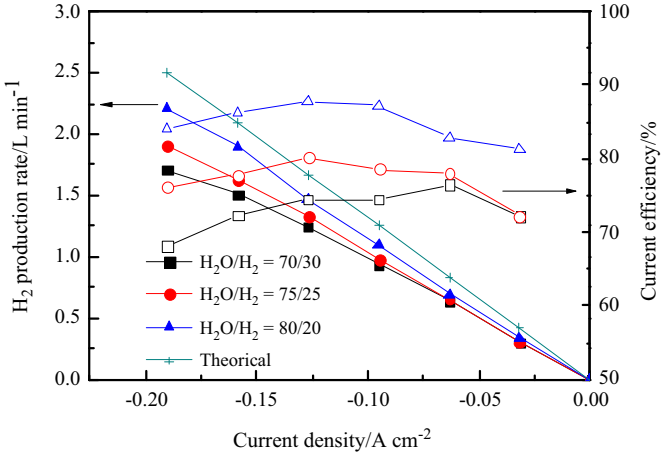

Fig. 8. Effect of different H_2O/H_2 ratios on the H_2 production rates and current efficiencies of the SOE stack module at 800 °C.

0.8 L min^{-1} hydrogen was supplied to the hydrogen electrode to maintain the reductive environment and act as an inlet carrier gas, this hydrogen rate should be deducted from the actual hydrogen production rate calculated for the stack module. Fig. 7 shows the hydrogen production performance of the stack module. In Fig. 7, the measured hydrogen production was calculated from the hydrogen flow rate directly measured at the outlet of the stack module, which differs from the actual hydrogen production because it also contains the carrier gas supplied to the hydrogen electrode. The actual hydrogen production was thus obtained in Fig. 7 by subtracting the measured hydrogen production at OCV from the measured hydrogen production at 0.15 A cm^{-2}. The outlet hydrogen flow rate at the OCV was measured 900 s prior to the beginning of galvanostatic electrolysis, and the average flow rate was found to be about 0.775 L min^{-1} instead of 0.8 L min^{-1}. This finding indicates that some hydrogen molecules either maintained the reductive environment or leaked out of the stack. The outlet hydrogen flow rate at 0.15 A cm^{-2} was also measured for 2700 s, and the average flow rate was found to be about 2.501 L min^{-1} (Fig. 7). The actual hydrogen production rate of the stack module was 1.726 L min^{-1}. Based on the ratio of the actual and theoretical hydrogen production rates, the current efficiency was calculated to be 87.4%, which indicates either current loss or hydrogen leakage in the stack.

Similar to the method used in Fig. 7, Fig. 8 shows the H_2 production rates and current efficiencies for the SOE stack module at different H_2O/H_2 ratios. In Fig. 8, the actual hydrogen production rate and current efficiency of the stack module increased with increasing H_2O/H_2 ratio. Increases in steam content resulted in increases in steam pressure, which promoted the uniform distribution of steam and increased the electrolysis current utilization rate. Thus, the actual hydrogen production rate increased with increasing H_2O/H_2 ratio in the SOE stack. In Fig. 8, the current efficiency first increased and then decreased at the same H_2O/H_2 ratio, which indicates that the current efficiency is similar to electrolysis efficiency which will decrease at high current density because of the Joule heat. Typical operating conditions for the 30-cell SOE stack modules are listed in Table 1.

Table 1
Typical operating conditions for the 30-cell SOE stack modules.

Stack module temperature (°C)	800
Average stack module voltage (V)	36–41
Stack module current (A)	9.45
Current density (A cm^{-2})	0.15
Hydrogen production rate (N L min^{-1}/N L h^{-1})	1.726/103.6
Inlet hydrogen (L min^{-1}/sccm cm^{-2})	0.8/0.42
Inlet steam (L min^{-1}/sccm cm^{-2})	3.2/1.68
Sweep air (L min^{1}/sccm cm^{-2})	12/6.3
Inlet steam mole fraction	0.80
Inlet hydrogen mole fraction	0.20
Steam conversion rate (%)	62
Electrolysis efficiency (%)	113–92
Current efficiency (%)	87.4

Degradation in the SOE stack module may be explained by several reasons. Post-mortem analysis was difficult to perform after electrolysis operation, and discernible changes in microstructure were observed in few cells and interconnect. Fig. 9 shows typical SEM microstructures of the cross-section of a few cells in the SOE stack module obtained after electrolysis. As shown in Figs. 9a and c, delamination of the LSM–YSZ oxygen electrode layer by the electrolyte may contribute to the degradation of the stack module. Interestingly, delamination mainly occurred in the steam and air inlet area of the 10×10 cm^2 cells, with delamination in the steam inlet area appearing even more severe than that in the air inlet area. SEM micrographs of the YSZ and LSM–YSZ surfaces after delamination are shown in Fig. 10 (peeled off LSM–YSZ from YSZ). The surface of the YSZ electrolyte was characterized by the formation of nanoparticles (Fig. 10a), and the nanoparticles were uniformly distributed on the YSZ surface. On the surface of the LSM–YSZ oxygen electrode in direct contact with the YSZ electrolyte, fine grains formed on the contact surface but no nanoparticles were found on the YSZ electrolyte surface (Fig. 10b). The nanoparticles formed on the YSZ electrolyte surface are most likely due to the migration or incorporation of oxygen ions from YSZ into LSM grains. Such incorporation

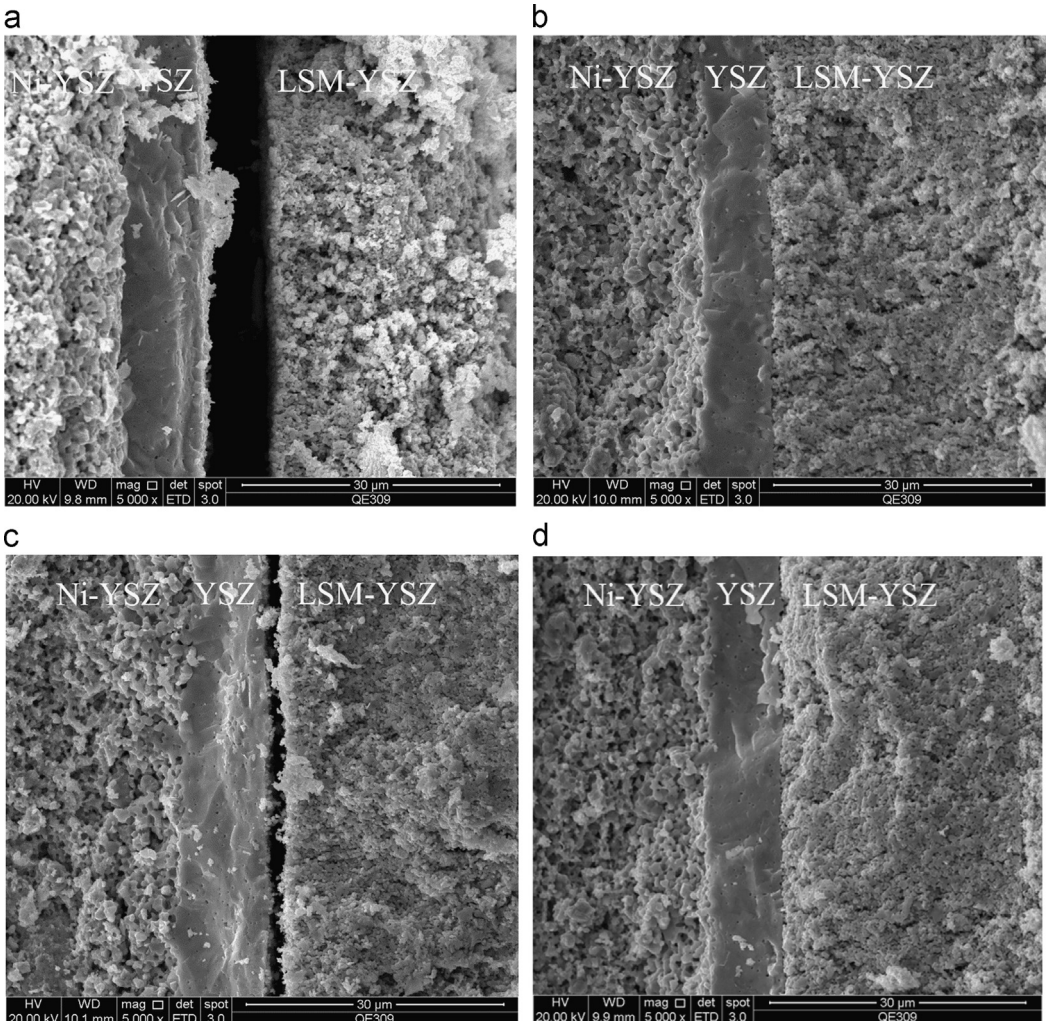

Fig. 9. SEM images of the cross-section (fracture surface) of the Ni-YSZ/YSZ/LSM–YSZ cells after electrolysis: (a) steam inlet area, (b) steam outlet area, (c) air inlet area, and (d) air outlet area.

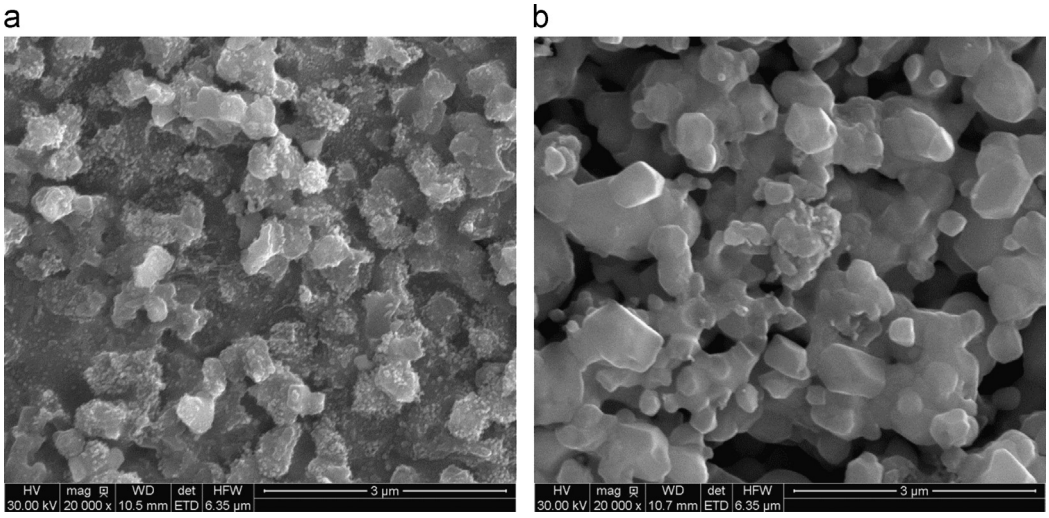

Fig. 10. SEM images of (a) the YSZ electrolyte surface in contact with the LSM–YSZ oxygen electrode and (b) the inner surface of the LSM–YSZ oxygen electrode in contact with the YSZ electrolyte after electrolysis.

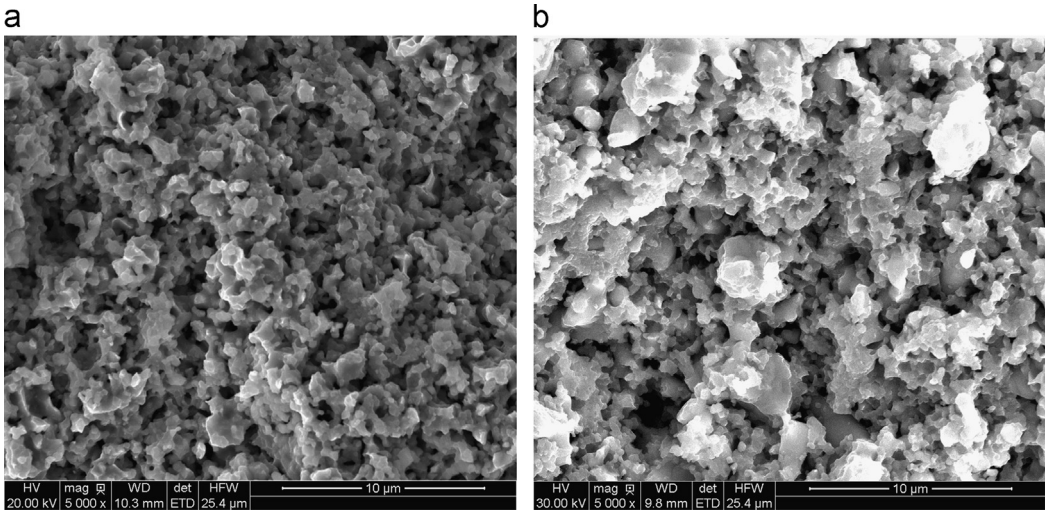

Fig. 11. SEM images of the Ni-YSZ hydrogen electrode (a) before and (b) after electrolysis.

leads to the shrinkage of the LSM lattice, which then induces local tensile strains within LSM particles and subsequent microcrack and nanoparticle cluster formation on the interface. More work will be necessary to understand the microstructural changes that occur within nanoparticles under SOE stack operation condition. The formation of nanoparticles may weaken the oxygen electrode/electrolyte interface, resulting in delamination of the LSM–YSZ oxygen electrode, especially in the steam and air inlet areas in the cells, under high internal partial pressures of oxygen.

Fig. 11 shows SEM microstructures of the Ni-YSZ hydrogen electrode before and after the electrolysis test. Compared with the microstructures of the hydrogen electrode before the test (Fig. 11a), slight agglomeration of Ni in the Ni-YSZ structure was observed, and the porosity of Ni-YSZ hydrogen electrode appeared to decrease after SOEC operation (Fig. 11b). Agglomeration of Ni resulted in a decrease in the electrochemical activity of the Ni-YSZ hydrogen electrode. The steam partial pressure exceeded 70% in the SOEC, and the diffusion process of steam was much more difficult than that of hydrogen. Consequently, the decrease in porosity increased the difficulty of the diffusion process for steam.

4. Conclusions

30-Cell SOE stack modules were manufactured and operated in steam electrolysis mode at 800 °C for hydrogen production under different operating conditions. The electrolysis efficiency, current efficiency, and actual hydrogen production rate of the stack modules increased with increasing H_2O/H_2 ratio at a constant current density. In addition, the electrolysis and current efficiencies decreased at high current densities. To achieve high hydrogen production rates with high electrolysis and current efficiencies at high H_2O/H_2 ratios, trade-offs among current density (hydrogen production rate), electrolysis efficiency, and current efficiency were observed. The stack modules were operated at 800 °C and a constant current density of 0.15 A cm^{-2} for hydrogen production for up to 1100 h with a steam conversion rate of 62%. The degradation rate was approximately 11.7% kh^{-1} and the electrolysis efficiency decreased from 113% to 92%. The actual hydrogen production rate of the 30-cell SOE stack modules reached 103.6 N L h^{-1} with a current efficiency of 87.4%. Post-mortem analysis showed that the main factors responsible for degradation of the SOE stack modules were delamination of the LSM–YSZ oxygen electrode occurring in the steam and air inlet areas of the 10 × 10 cm^2 cells, slight agglomeration of Ni, decreases in the porosity of the Ni-YSZ hydrogen electrode.

Acknowledgments

This work was supported by China Postdoctoral Science Foundation (2012M521208), Zhejiang Provincial Advanced Postdoctoral Scientific Program (Bsh1201010), Ningbo Natural Science Foundation (2013A610028), Chinese Academy of Sciences (Project Position kgcx2-yw-314), and National High-Tech Research and Development Program of China (863 Project no. 2011AA050703).

References

[1] M. Ni, M.K.H. Leung, D.Y.C. Leung, K. Sumathy, A review and recent developments in photocatalytic water-splitting using TiO_2 for hydrogen production, Renew. Sustain. Energy Rev. 11 (2007) 401–425.
[2] M. Ni, D.Y.C. Leung, M.K.H. Leung, K. Sumathy, An overview of hydrogen production from biomass, Fuel Process. Technol. 87 (2006) 461–472.
[3] M. Fishcher, Review of hydrogen production with photovoltaic electrolysis systems, Int. J. Hydrog. Energy 11 (1986) 495–501.
[4] M.A. Laguna-Bercero, Recent advances in high temperature electrolysis using solid oxide fuel cells: a review, J. Power Sources 203 (2012) 4–16.
[5] C. Jin, C.H. Yang, F. Zhao, D.A. Cui, F.L. Chen, $La_{0.75}Sr_{0.25}Cr_{0.5}Mn_{0.5}O_3$ as hydrogen electrode for solid oxide electrolysis cells, Int. J. Hydrog. Energy 36 (2011) 3340–3346.
[6] S.D. Kim, J.H. Yu, D.W. Seo, I.S. Han, S.K. Woo, Hydrogen production performance of 3-cell flat-tubular solid oxide electrolysis stack, Int. J. Hydrog. Energy 37 (2012) 78–83.

[7] X.Y. Zhang, J.E. O'Brien, R.C. O'Brien, G.K. Housley, Durability evaluation of reversible solid oxide cells, J. Power Sources 242 (2013) 566–574.
[8] Y. Gan, Q.Q. Qin, S.G. Chen, Y. Wang, D.H. Dong, K. Xie, Y.C. Wu, Composite cathode $La_{0.4}Sr_{0.4}TiO_{3-\delta}$–$Ce_{0.8}Sm_{0.2}O_{2-\delta}$ impregnated with Ni for high-temperature steam electrolysis, J. Power Sources 245 (2014) 245–255.
[9] C.M. Stoots, J.E. O'Brien, K.G. Condie, J.J. Hartvigsen, High-temperature electrolysis for large-scale hydrogen production from nuclear energy – experimental investigations, Int. J. Hydrog. Energy 35 (2010) 4861–4870.
[10] Z.W. Wang, M. Mori, T. Araki, Steam electrolysis performance of intermediate-temperature solid oxide electrolysis cell and efficiency of hydrogen production system at 300 $Nm^3\,h^{-1}$, Int. J. Hydrog. Energy 35 (2010) 4451–4458.
[11] Y. Chen, J. Bunch, T.S. Li, Z.P. Mao, F.L. Chen, Novel functionally graded acicular electrode for solid oxide cells fabricated by the freeze-tape-casting process, J. Power Sources 213 (2012) 93–99.
[12] S.C. Singhal, Solid oxide fuel cells for stationary, mobile, and military applications, Solid State Ion. 152–153 (2002) 405–410.
[13] C. Yang, C. Jin, F. Chen, Micro-tubular solid oxide fuel cells fabricated by phase-inversion method, Electrochem. Commun. 12 (2010) 657–660.
[14] C. Jin, C. Yang, F. Chen, Effects on microstructure of NiO–YSZ anode support fabricated by phase-inversion method, J. Membr. Sci. 363 (2010) 250–255.
[15] S.H. Jensen, P.H. Larsen, M. Mogensen, Hydrogen and synthetic fuel production from renewable energy source, Int. J. Hydrog. Energy 32 (2007) 3253–3257.
[16] A. Hauch, S.H. Jensen, S. Ramousse, M. Mogensen, Performance and durability of solid oxide electrolysis cells, J. Electrochem. Soc. 153 (2006) A1741–A1747.
[17] A. Brisse, J. Schefold, M. Zahid, High temperature water electrolysis in solid oxide cells, Int. J. Hydrog. Energy 33 (2008) 5375–5382.
[18] J. Kim, H.I. Ji, H.P. Dasari, D. Shin, H. Song, J.H. Lee, B.K. Kim, H.J. Je, H.W. Lee, K.J. Yoon, Degradation mechanism of electrolyte and air electrode in solid oxide electrolysis cells operating at high polarization, Int. J. Hydrog. Energy 38 (2013) 1225–1235.
[19] M. Petitjean, M. Reytier, A. Chatroux, L. Bruguiere, A. Mansuy, H. Sassoulas, S.D. Iorio, B. Morel, J. Mougin, Performance and durability of high temperature steam electrolysis: from single cell to short-stack scale, ECS Trans. 35 (2011) 2905–2913.
[20] W.B. Guan, H.J. Zhai, L. Jin, T.S. Li, W.G. Wang, Effect of contact between electrode and interconnect on performance of SOFC stacks, Fuel Cells 11 (2011) 445–450.
[21] W.B. Guan, H.J. Zhai, L. Jin, C. Xu, W.G. Wang, Temperature measurement and distribution inside planar SOFC stacks, Fuel Cells 12 (2012) 24–31.
[22] L. Jin, W.B. Guan, X. Ma, C. Xu, W.G. Wang, Achieving hydrogen production through solid oxide electrolyzer stack by high temperature electrolysis, ECS Trans. 41 (2012) 103–111.
[23] S.D. Ebbesen, J. Høgh, K.A. Nielsen, J.U. Nielsen, M. Mogensen, Durable SOC stacks for production of hydrogen and synthesis gas by high temperature electrolysis, Int. J. Hydrog. Energy 36 (2011) 7363–7373.
[24] Q. Cai, E. Luna-Ortiz, C.S. Adjiman, N.P. Brandon, The effects of operating conditions on the performance of a solid oxide steam electrolyser: a model-based study, Fuel Cells 10 (2010) 1114–1128.
[25] J.E. O'Brien, C.M. Stoots, J.S. Herring, M.G. McKellar, E.A. Harvego, M.S. Sohal, K.G. Condie, High temperature electrolysis for hydrogen production from nuclear energy – technology summary, Idaho National Laboratory, February 2010.
[26] R.M. Xing, Y.R. Wang, S.H. Liu, C. Jin, Preparation and characterization of $La_{0.75}Sr_{0.25}Cr_{0.5}Mn_{0.5}O_{3-\delta}$–yttria stabilized zirconia cathode supported solid oxide electrolysis cells for hydrogen generation, J. Power Sources 208 (2012) 276–281.
[27] C.H. Yang, C. Jin, A. Coffin, F.L. Chen, Characterization of infiltrated $(La_{0.75}Sr_{0.25})_{0.95}MnO_3$ as oxygen electrode for solid oxide electrolysis cells, Int. J. Hydrog. Energy 35 (2010) 5187–5193.
[28] A. Brisse, J. Schefold, M. Zahid, High temperature water electrolysis in solid oxide cells, Int. J. Hydrog. Energy 33 (2008) 5375–5382.
[29] M.A. Laguna-Bercero, R. Campana, A. Larrea, J.A. Kilner, V.M. Orera, Performance and aging of microtubular YSZ-based solid oxide regenerative Fuel Cells, Fuel Cells 11 (2011) 116–123.
[30] C.H. Yang, A. Coffin, F.L. Chen, High temperature solid oxide electrolysis cell employing porous structured $(La_{0.75}Sr_{0.25})_{0.95}MnO_3$ with enhanced oxygen electrode performance, Int. J. Hydrog. Energy 35 (2010) 3221–3226.
[31] T. Ishihara, T. Kannou, Intermediate temperature steam electrolysis using $LaGaO_3$-based electrolyte, Solid State Ion. 192 (2011) 642–644.
[32] J. Schefold, A. Brisse, M. Zahid, J.P. Ouweltjes, J.U. Nielsen, Long term testing of short stacks with solid oxide cells for water electrolysis, ECS Trans. 35 (2011) 2915–2927.